Electrical Power and Energy Systems 104 (2019) 593–602

Contents lists available at ScienceDirect

Electrical Power and Energy Systems

journal homepage: www.elsevier.com/locate/ijepes

Distributed cooperative voltage control of wind farms based on consensus protocol

Yifei Guo, Houlei Gao*, Qiuwei Wu

Key Laboratory of Power System Intelligent Dispatch and Control of Ministry of Education, Shandong University, China

ARTICLE INFO

Keyword:
Consensus protocol
Reactive power
Voltage control
Wind farm

ABSTRACT

The increasing penetration level of wind power brings a number of challenges to power system operations. Voltage/reactive power control is an important task of a wind farm to fulfill the grid requirements and avoid the cascading trip faults of wind turbines (WTs). To address this issue, a distributed cooperative voltage control strategy is proposed for wind farms based on the consensus protocol in this paper. In the proposed voltage control scheme, a droop-based local controller is adopted for the primary voltage control based on the local measurements. A consensus-based distributed secondary voltage controller is proposed, aiming to regulate the voltages within the feasible range while optimizing reactive power sharing among the reactive power sources using the local and neighboring information. The controller parameters are determined by the closed-loop system stability analysis using a linearized model. A wind farm with 20 WTs was used for the case study to validate the proposed control scheme under both steady-state and fault-ride-through (FRT) conditions. Moreover, the robustness against a communication link failure and plug-and-play capability of the proposed voltage controller were tested.

1. Introduction

Wind energy has become one of the most important and promising renewable energy in last few years due to the growing public concerns with energy shortage and environment. According to the global wind statistics provided by the Global Wind Energy Council (GWEC), the new installed wind capacity in 2017 is 53 GW and the global cumulative installed capacity has reached up to 540 GW by the end of 2017 [1]. The rolling five year forecast sees the cumulative installed capacity will be over 800 GW by the end of 2021 [2].

The fast increasing penetration of wind power has brought a number of technical and economic challenges to power system planning and operation due to its uncertainty and variability [3,4]. A number of new technical requirements and grid codes for wind power integration have been introduced by system operators and regulators [5,6]. The modern wind farms are required to be equipped with voltage and reactive power control system and consequently can regulate the voltage at the point of connection (POC) within a specific range to mitigate the negative effects induced by intermittent wind power. Besides, terminal voltages of wind turbines (WTs) should be also maintained within the feasible range to avoid cascading trip-off failures of WTs.

Centralized voltage control schemes have been widely investigated. In [7,8], the total required reactive power of wind farms is calculated according to the voltage at the POC based on the proportional-integral (PI) control loop and then dispatched to each WT based on the proportional distribution according to their the available reactive power capacity. In recent years, the optimization-based coordinated voltage control strategies are widely studied, in which voltage control problems are formulated as an optimization problem and solved by the central controllers every few seconds [9–15]. In [9], a hierarchical automatic voltage control (AVC) for wind farms was designed and implemented in a large-scale wind pool area of Northern China. Three different control modes were designed for different operating requirements ranked by the priority: 1) corrective mode, which aims to regulate the terminal voltage of WTs; 2) coordinated mode, which aims to track the reference sent from the control center while mitigating voltage fluctuations considering operation constraints; 3) preventive mode, in which the dynamic reactive power reserve is optimized while the voltage profile is controlled within the feasible range. In [10], a model predictive control (MPC) based coordinated voltage control scheme was proposed to coordinate various voltage regulation devices with different response time including WTs, Static Var Compensators (SVCs) and on-load tap changing (OLTC) transformers. As an extension of [10], a combined active and reactive power control strategy was proposed to take into account the effects of active power control on voltage profile considering the high R/X ratio of the wind farm collector system [11]. In [12], an

* Corresponding author.
E-mail address: houleig@sdu.edu.cn (H. Gao).

https://doi.org/10.1016/j.ijepes.2018.07.030
Received 29 March 2018; Received in revised form 20 June 2018; Accepted 16 July 2018
Available online 26 July 2018
0142-0615/

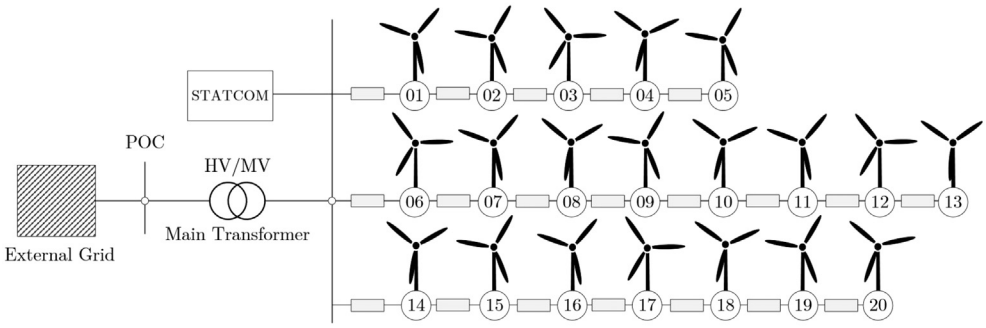

Fig. 1. The typical structure of a wind farm.

optimal power flow (OPF)-based reactive power dispatch method was proposed to reduce the electrical losses inside offshore wind farms including not only the losses in cables and transformers but also in WTs and HVDC converters. In [13], a two-layer voltage control scheme for offshore wind farms was designed which combines the optimization-based method and a PI controller. In the upper layer, the offline OPF calculation is executed every several minutes to determine the voltage reference of the pilot bus and then a PI controller is used to track the voltage reference in the lower layer. In [14,15], the MPC-based voltage control strategies for offshore HVDC connected wind farms were proposed to regulate the voltage across the offshore networks by optimally coordinating the HVDC converter and WTs. In [16], an optimization-based approach to couple AVC system to the market price was proposed in order to accurately evaluate the operation cost, where the control objective is to minimize the operation cost including the grid loss, the shunt switching cost, the tap change cost and the cost of voltage control service provided by the power plant owners.

The centralized voltage control strategies can guarantee the optimal control performance based on the global information. However, they might not be suitable for the future large-scale wind farms with several hundred or even thousands of WTs due to the limitations as follows: i) The computation burden of central controllers dramatically grows with the increasing number of WTs [18]. ii) In terms of cost, the centralized control schemes require complicated communication networks to acquire the remote information (voltage, power, etc.) at each bus, indicating that there will be a huge investment of communication infrastructures for a large-scale wind farm [19–21]. iii) The control performance highly depends on the properties and reliability of the communication systems and central controller without adequate robustness and flexibility [18,21,22]. iv) The optimization-based methods are designed with the control period of several seconds or even minutes [9–15] with slow response time. Hence, they might fail to handle the ultra short-term voltage issue with the time-scale of milliseconds such as the fault-ride-through (FRT) control.

The distributed control technique has been rapidly developed in recent years, which is widely used in voltage and frequency control of smart microgrids and distribution networks [17–24]. The distributed active power dispatch strategies of wind farms have been investigated, which aim to minimize the fatigue loads of WTs while tracking the active power reference set by system operators [28–30]. [25,26], decentralized (local) voltage control schemes were designed based on the local information without coordination. In [27], the stability boundaries of decentralized voltage control were investigated. For the local voltage control, once the estimation of the system parameters is poor, it can lead to reactive power oscillations and voltage flicker caused by unwanted interaction between individual control loops [27]. Moreover, the local control only addressed on voltage performance without considering the fair reactive power sharing.

In this paper, a distributed cooperative voltage control strategy (DCVCS) is proposed for wind farms based on the consensus protocol. A droop-based local voltage controller is designed as the primary control of WTs and Static Synchronous Compensators (STATCOMs) to achieve fast response. A consensus-based distributed secondary voltage controller is designed to mitigate the steady-state voltage deviations generated by droop controllers while maintaining fair reactive power sharing among the reactive power sources using the local and neighboring information. The small-signal stability analysis of the closed-loop system is performed based on a linearized model. Compared with the centralized control strategies, the proposed DCVCS has several advantages as follows: i) It is center-free, eliminating the requirement of a central (supervisor) controller. ii) It consists of two layers: primary control and secondary control. The primary control is carried out based on the local voltage measurements to provide fast response especially under emergency conditions and the secondary control is performed to improve the voltage performance and achieve fair reactive power sharing, which only requires information exchange with its immediate neighbors, largely reducing the cost of the communication infrastructures. iv) It eliminates the requirements of the network parameters and implying better robustness against network changes. Compared with the pure local control, the proposed scheme can avoid the closed-loop instability by properly selecting control parameters and address the fair reactive power sharing issue.

The rest of this paper is organized as follows. Section 2 gives an overview of the proposed DCVCS. In Section 3, the droop-based primary voltage controller is presented. In Section 4, the consensus-based distributed cooperative secondary voltage controller is proposed. Section 5 presents the stability analysis of the close-loop system based on a linearized model. In Section 6, the simulation results and discussions are presented, followed conclusions.

2. Overview of the distributed cooperative voltage control scheme of a wind farm

2.1. Problem description

The typical structure of a wind farm with 20 WTs is illustrated in Fig. 1. The wind farm as shown in Fig. 1 with 20 × 5 MW full-converter (FC)-WTs and 1 × ±20 MVar STATCOM is considered. The WTs are connected by three 33 kV feeders and placed with a distance of 1.5 km between two adjacent WTs. The STATCOM is placed at the MV side of the main transformer to provide reactive power support for the wind farm. For simplification, the set of reactive power source including WTs and the STATCOM are denoted together by the set $\mathcal{I}$. All WTs and the STATCOM should be cooperatively controlled to achieve the following objectives:1) The voltage profile across the wind farm network including the voltage at POC and WT buses should be controlled around the voltage reference V^*,

$$V \to V^*. \tag{1}$$

Generally, for the WT terminal voltage, they should be controlled within the deviations of 0.07–0.08 p.u. to avoid be tripped by the protection configuration (generally 0.9–1.1 p.u.) [9]. For the POC, the

voltage should be controlled to fulfill certain grid requirements, such as 0.97–1.03 p.u. required by State Grid Corporation of China.2) Each reactive power source (WTs or STATCOM) is treated equally with a common reactive power utilization ratio ξ^*, i.e.,

$$\xi \to \xi^* \tag{2}$$

with $\xi_i = Q_i/\overline{Q}_i$, $\forall\, i \in \mathscr{I}$. Q_i and $\overline{Q}_i$ are the generated and available reactive power of unit i. For a full-converter based WT, the available reactive power can be given by $\overline{Q}_W = \sqrt{(S_W)^2-(P_W)^2}$ [13] where S_W is the MVA rating of the WT. This control objective aims to keep fair reactive power sharing within the wind farm.

For a FC-WT, the grid side converter is controlled to provide reactive support which is achieved via a decoupled control structure including the inner current loop and outer voltage loop. For the reactive power loop, the constant Q control mode is adopted, of which the command signal is sent from the proposed controller. Similarly, the STATCOM also operates with the constant Q mode in this study. More details of the WT and STATCOM modeling can be referred to [31–34].

2.2. Primary and secondary voltage control design

The structure of the control system is illustrated in Fig. 2. The $Q-V$ droop control is designed as the primary voltage control only based on the local information, which can provide fast reactive power support. Each WT directly regulates its own terminal voltage and the voltage at the POC is directly regulated by the STATCOM. The secondary voltage control is developed based on the distributed averaging-consensus protocol, which generates an additional incremental control command q to the primary controller. In the secondary control, each unit only exchanges information with their immediate neighbors. The basic mechanism of the two-layer voltage control can be briefly shown by Fig. 3. To clearly explain this mechanism, the reactive sharing is not considered here. Without the secondary control, the units operates based on the droop rule (solid line) and suppose (Q, V) is the equilibrium with the voltage deviation V^*-V. To mitigate the voltage deviation, the secondary controller ensures the voltage restore to the reference V^* (dotted line) by adjusting the reactive power from Q to Q'. Similarly, the secondary control for reactive power sharing can also be explained as above.

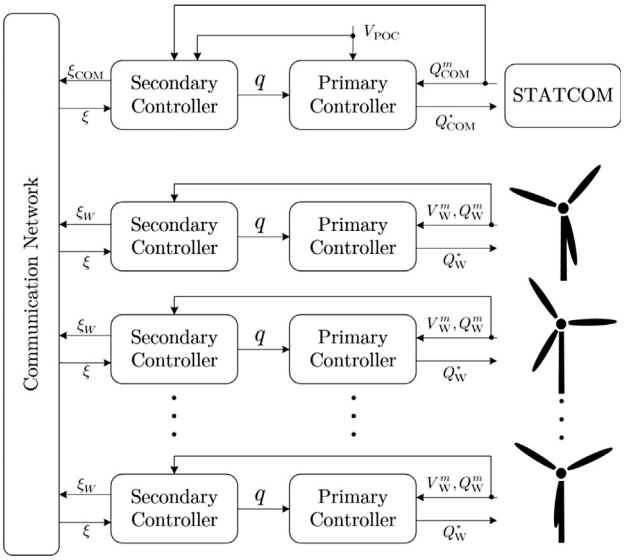

Fig. 2. Structure of the proposed distributed cooperative voltage control strategy.

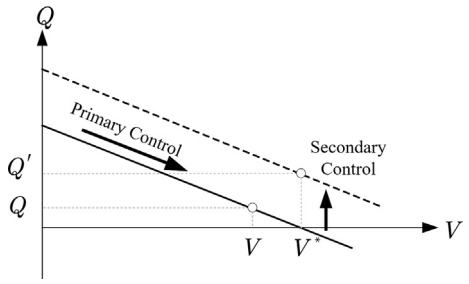

Fig. 3. Schematic diagram of primary and secondary voltage control.

3. Primary voltage control

To realize the fast response capability of the voltage control system, local droop control is adopted in this scheme for the primary control. It utilizes the fact that the voltage magnitude difference depends predominantly on reactive power. Its basic function is providing reactive power references for WTs and STATCOM according to the measured voltage. The voltage droop controller specifies the reactive power injection Q_i^* by,

$$Q_i^*(t) = -K_i(V_i^m(t)-V^*(t)) + Q_i^{\mathrm{set}} \tag{3}$$

where V_i^m is the local measured voltage of unit i;K_i is the droop coefficient; Q_i^{set} is the reactive power set-point. Here, we consider $Q_i^{\mathrm{set}} = 0$. The measured voltage V_i^m can be obtained through the following first-order low pass filters as [24],

$$\tau_m \dot{V}_i^m(t) = -V_i^m(t) + V_i(t) \tag{4}$$

where τ_m denotes the time constant of the filter and V_i is the actual voltage.

4. Secondary voltage control

Basically, the secondary voltage control is used to eliminate the voltage deviations generated by the droop controller. Moreover, the fair reactive power sharing is considered in the secondary control.

4.1. Preliminaries—consensus problem on graphs

The topology of a communication network can be described by a weighted graph $\mathscr{G} = (\mathscr{V}, \mathscr{E}, \mathscr{A})$ where $\mathscr{V} = \{v_1, \ldots, v_n\}$ denotes the set of nodes with the finite node index set $\mathscr{I} = 1, 2, \ldots, n$, $\mathscr{E} \subseteq \mathscr{V} \times \mathscr{V}$ is set of edges, and $\mathscr{A} = [a_{ij}] \in \mathbb{R}^{n\times n}$ is the weighted adjacency matrix with elements $a_{ij} = a_{ji} > 0$. An edge is denoted by $e_{ij} = (v_i, v_j)$ and thus $e_{ij} \in \mathscr{E} \Leftrightarrow a_{ij} > 0$. The neighboring nodes set of node i is denoted by $\mathscr{N}_i = \{j | (i, j) \in \mathscr{E}\}$. The Laplacian matrix of the graph is defined as $\mathscr{L} = \mathscr{D}-\mathscr{A}$, where $\mathscr{D} = \mathrm{diag}(d_1, \ldots, d_n) \in \mathbb{R}^{n\times n}$ is the in-degree matrix with elements $d_i = \sum_{j\in\mathscr{N}_i} a_{ij}$.

Let $x \in \mathbb{R}$ be the value of the node i. A commonly studied continuous-time averaging-consensus protocol is as follows [35]:

$$\dot{x}_i(t) = -\sum_{j=1}^{n} a_{ij}(x_i(t)-x_j(t)),\ \forall\, i, j \in \mathscr{I} \tag{5}$$

According to the theorem in [35], the value of node i is adjusted by the update rule. If the graph $\mathscr{G}$ is connected, the dynamic process will converge to a stable equilibrium $x_1(\infty) = \cdots = x_n(\infty) = 1/n(\sum_{i=1}^{n} x_i(0))$.

4.2. Communication network design

As mentioned above, the basic requirement of the communication network is that the graph must be a connected graph, i.e., there must be a path in the communication graph between any two nodes. Moreover, to enhance the robustness of the communication network, all the possible "$N-1$" scenarios are considered in the communication network

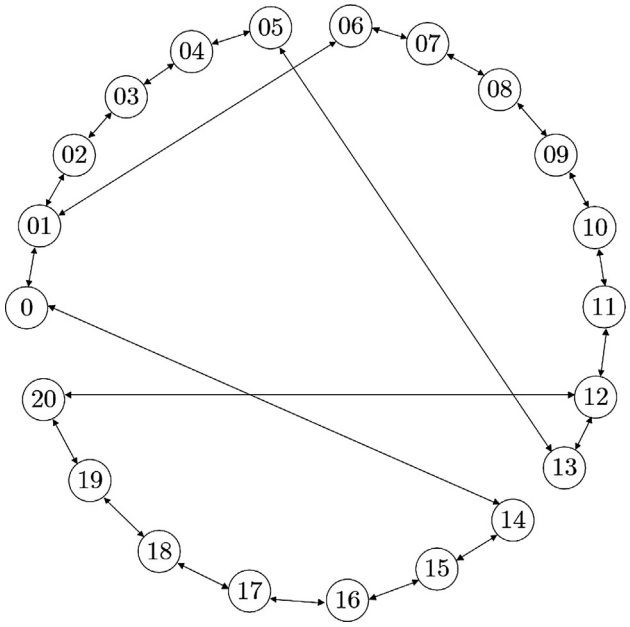

Fig. 4. Topology of the communication network. (The STATCOM is numbered by the Node 0 and WT01–WT20 are sequentially numbered by the Node 01–Node 20.)

design. Hence, firstly, the network design problem can be transformed into a minimum spanning tree problem and can be solved by the Prim algorithm [36]. The geographic distance between any two units is considered as the measure of the communication construction cost. Accordingly, based on the wind farm configuration in Fig. 1, the communication network topology is illustrated in Fig. 4. In this graph, in addition to the minimum spanning tree, two extra communication links (05, 13) and (12, 20) are designed to guarantee the connectivity of the communication network considering any one "$N-1$" scenario.

4.3. Distributed cooperative secondary voltage control based on consensus protocol

Similar to the automatic generation control of bulk systems, the secondary voltage control of a wind farm is used to compensate the voltage deviations as shown in Fig. 3.

Hence, a consensus-based secondary voltage control is implemented by adding the control input q_i, $\forall\, i \in \mathscr{I}$, to the primary droop controller, which is expressed as,

$$\begin{cases} Q_i^*(t) = & -K_i(V_i^m(t) - V^*(t)) + q_i(t) \\ \lambda_i \dot{q}_i(t) = & -\alpha_i(V_i^m(t) - V^*(t)) \\ & -\beta_i \sum_{j=1}^{n} a_{ij}(V_i^m(t) - V_j^m(t)) \\ & -\gamma_i \sum_{j=1}^{n} a_{ij}\left(\frac{Q_i^m(t)}{\bar{Q}_i(t)} - \frac{Q_j^m(t)}{\bar{Q}_j(t)}\right) \end{cases} \tag{6}$$

Q_i^m is the measured reactive power output which is obtained through the low pass filter with the time constant of τ_m. $\lambda_i > 0$, $\alpha_i \geqslant 0$, $\beta_i \geqslant 0$ and $\gamma_i \geqslant 0$ are the constant gains. At the right side of the second equation, the first and second terms are designed for mitigating voltage deviations whereas the third one is used for regulating reactive power sharing. In this paper, the adjacent matrix $\mathscr{A}$ is defined using a standard form, i.e., $a_{ij} = 1$ if $e_{ij} \in \mathscr{E}$, otherwise $a_{ij} = 0$. Actually, from (6), it can be concluded that, the impact of different selection of a_{ij} on system dynamics is nearly equivalent to that of the parameters β, γ, or λ. For instance, increasing a_{ij} has an effect nearly identical to increasing β, γ or decreasing λ. The impact of parameters β, γ and λ will be discussed later and we therefore omit the discussion of different a_{ij}.

There is a tradeoff between voltage regulation and reactive power sharing due to their conflicts. If $\gamma_i = 0$ for all nodes $i \in \mathscr{V}$, it would be a pure voltage controller and all bus voltages can accurately converge to the reference value in finite time. If $\alpha_i = 0$ and $\beta_i = 0$ for all nodes $i \in \mathscr{V}$, it will result in accurately fair reactive power sharing but the voltages cannot be effectively controlled at the nominal value.

5. Stability analysis

Obviously, the closed-loop system including the physical network and control loops is a highly nonlinear system. In this section, we present a small-signal stability analysis based on a linearized model and investigate the effects of several control parameters on system stability in order to better design the controller.

5.1. Modeling

5.1.1. WT and STATCOM

The FC-WT and voltage-source-converter (VSC)-based STATCOM have the similar control strategy with a cascading control structure, i.e., outer voltage control loop and inner current control loop. The control loop is faster than the droop control and secondary control. To avoid unnecessary technical complications, we model any time delay in adjusting the output reactive power of WTs and STATCOM with a simple first-order function with a time constant τ_{Q_i}, i.e.,

$$\tau_{Q_i}\dot{Q}_i(t) = -Q_i(t) + Q_i^*(t). \tag{7}$$

5.1.2. Network

In this study, we consider the network consisting of N buses and the set is defined as $\mathscr{B} = \{1, 2, ..., N\}$. Based on the assumption that the voltage magnitude is strongly related to the reactive power, the reactive power balance relation can be generally expressed as,

$$Q_{G_i} - Q_{L_i} = -V_i \sum_{i=1}^{N} V_j B_{\text{bus}}(i,j),\ \forall\ i,j \in \mathscr{B} \tag{8}$$

where Q_{G_i} and Q_{L_i} denote the generated reactive power and reactive power load at bus i, respectively; $B_{\text{bus}} \in \mathbb{R}^{N\times N}$ denotes the susceptance matrix. Suppose there is no extra reactive power load inside the wind farm, i.e., $Q_{L_i} = 0$, and replace Q_{G_i} by Q_i, $\forall\ i \in \mathscr{B}$, the network model can be written into a compact form,

$$Q = -[V]B_{\text{bus}}V \tag{9}$$

where $Q = [Q_1, ..., Q_N]^\top \in \mathbb{R}^{N\times 1}$, $V = [V_1, ..., V_N]^\top \in \mathbb{R}^{N\times 1}$. Here, $[*]$ denotes the diagonal matrix with the vector $*$ along the diagonal. For instance, $[V] = \text{diag}(V_1, ..., V_N)$.

5.2. Linearized model of the closed-loop system

Without loss of generality, suppose the network includes N_K slack/PV buses, N_S PQ buses equipped with reactive power source (WT or STATCOM), and N_L pure load buses without reactive power source (i.e., $N = N_K + N_S + N_L$, $\mathscr{B} = \mathscr{B}_K \cup \mathscr{B}_S \cup \mathscr{B}_L$, $\mathscr{B}_K \cap \mathscr{B}_S = \varnothing$, $\mathscr{B}_K \cap \mathscr{B}_L = \varnothing$, and $\mathscr{B}_S \cap \mathscr{B}_L = \varnothing$). The voltage and reactive power vectors are partitioned according to the types of buses distinguished by the subscripts 'K', 'S', and 'L', respectively,

$$Q = \begin{bmatrix} Q_K \\ Q_S \\ \mathbf{0}_{N_L\times 1} \end{bmatrix}, \quad V = \begin{bmatrix} V_K \\ V_S \\ V_L \end{bmatrix}, \tag{10}$$

where $V_K \in \mathbb{R}^{N_K\times 1}$, $V_S \in \mathbb{R}^{N_S\times 1}$ and $V_L \in \mathbb{R}^{N_L\times 1}$ denote the corresponding voltage vectors of three types of buses, respectively; $Q_K \in \mathbb{R}^{N_K\times 1}$ and $Q_S \in \mathbb{R}^{N_S\times 1}$ denote the corresponding reactive power injection vectors. $\mathbf{0}$ is the zero matrix. Besides, the susceptance matrix should be also

partitioned as,

$$B_{\text{bus}} = \begin{bmatrix} B_{KK} & B_{KS} & B_{KL} \\ B_{SK} & B_{SS} & B_{SL} \\ B_{LK} & B_{LS} & B_{LL} \end{bmatrix}. \tag{11}$$

Suppose the operating point is $V = V^0$, the linear relation can be obtained as,

$$V_S = -\underline{B}_{SS}[V_S^0]^{-1}Q_S - \underline{B}_{SS}^{-1}\underline{B}_{SK}V_K \tag{12}$$

where the reduced susceptance matrixes $\underline{B}_{SS} \in \mathbb{R}^{N_S \times N_S}$ and $\underline{B}_{SK} \in \mathbb{R}^{N_S \times N_K}$ are defined by,

$$\underline{B}_{SS} := B_{SS} - B_{SL}B_{LL}^{-1}B_{LS}, \tag{13}$$

$$\underline{B}_{SK} := B_{SK} - B_{SL}B_{LL}^{-1}B_{LK}. \tag{14}$$

Rewrite (6) and (7) into a compact form as,

$$\begin{cases} Q_S^*(t) = & -[K](V^m(t) - V^*(t)\cdot\mathbf{1}_{N_S\times 1}) + q(t) \\ [\lambda]\dot{q}(t) = & -[\alpha](V^m(t) - V^*(t)\cdot\mathbf{1}_{N_S\times 1}) \\ & -[\beta]\mathscr{L}V^m(t) - [\gamma]\mathscr{L}[\overline{Q}_S(t)]^{-1}Q_S \end{cases} \tag{15}$$

$$[\tau_Q]\dot{Q}_S(t) = -Q_S(t) + Q_S^*(t). \tag{16}$$

where
$K = [K_1, ..., K_{N_S}]^\top \in \mathbb{R}^{N_S\times 1}$, $\lambda = [\lambda_1, ..., \lambda_{N_S}]^\top \in \mathbb{R}^{N_S\times 1}$, $\alpha = [\alpha_1, ..., \alpha_{N_S}]^\top$, $\in \mathbb{R}^{N_S\times 1}$, $\beta = [\beta_1, ..., \beta_{N_S}]^\top \in \mathbb{R}^{N_S\times 1}$
$\gamma = [\gamma_1, ..., \gamma_{N_S}]^\top \in \mathbb{R}^{N_S\times 1}$, $\tau_Q = [\tau_{Q_1}, ..., \tau_{Q_{N_S}}]^\top \in \mathbb{R}^{N_S\times 1}$, $Q_S = [Q_{S_1}, ..., Q_{S_{N_S}}]^\top \in \mathbb{R}^{N_S\times 1}$,
$\overline{Q}_S = [\overline{Q}_{S_1}, ..., \overline{Q}_{S_{N_S}}]^\top \in \mathbb{R}^{N_S\times 1}$, $\mathbf{1}_{N_S\times 1} = [1, ..., 1]^\top \in \mathbb{R}^{N_S\times 1}$.

Assuming the available reactive power $\overline{Q}_i$, $i \in \mathscr{I}$ could not sharply change around the operating point, the linearized model of closed-loop system is obtained by substituting (12) and (16) into (15),

$$\dot{x}(t) = Ax(t) + Bu(t) \tag{17}$$

where

$$x = \begin{bmatrix} \dot{Q}_S \\ Q_S \\ \dot{q} \\ q \end{bmatrix} \in \mathbb{R}^{4N_S\times 1}, \quad u = \begin{bmatrix} V^* \\ V_K \end{bmatrix} \in \mathbb{R}^{(N_S+N_K)\times 1},$$

$$A = \begin{bmatrix} A_{11} & A_{12} & A_{13} & A_{14} \\ I_{N_S} & \mathbf{0}_{N_S\times N_S} & \mathbf{0}_{N_S\times N_S} & \mathbf{0}_{N_S\times N_S} \\ \mathbf{0}_{N_S\times N_S} & A_{32} & A_{33} & \mathbf{0}_{N_S\times N_S} \\ \mathbf{0}_{N_S\times N_S} & \mathbf{0}_{N_S\times N_S} & I_{N_S} & \mathbf{0}_{N_S\times N_S} \end{bmatrix} \in \mathbb{R}^{4N_S\times 4N_S},$$

$$B = \begin{bmatrix} B_{11} & B_{12} \\ \mathbf{0}_{N_S\times N_S} & \mathbf{0}_{N_S\times N_K} \\ B_{31} & B_{32} \\ \mathbf{0}_{N_S\times N_S} & \mathbf{0}_{N_S\times N_K} \end{bmatrix} \in \mathbb{R}^{4N_S\times(N_S+N_K)},$$

where I is the identity matrix. The sub-matrixes A_{11}, A_{12}, A_{13}, A_{14}, A_{32}, A_{33}, B_{11}, B_{12}, B_{31}, and B_{32} are presented in the Appendix.

5.3. Stability analysis

The system stability can be investigated based on the linearized model, which highly depends on the control parameters. The configuration of the wind farm has been presented in Section 2 with the communication network shown in Fig. 4. The time constant τ_Q of WTs and STATCOMs are designed as 0.1s and 0.03s. τ_m is 0.016s. For simplification, the parameters α, β, γ and λ are taken as uniform values. Moreover, considering the voltage profile is controlled around the reference V^*, the operating point is selected as $V_S^0 = V^*$.

The stability is evaluated based on the eigenvalues of the linearized system. It is impractical to show all root locus of the linearized system since it is high-order system. Here, the approximate conservative range of the parameters are illustrated in Table 1, which is helpful to design the controller. The analysis of each parameter is done independently and in a incremental way around the nominal values $\alpha^* = 1$, $\beta^* = 1$, $\gamma^* = 1$ and $\lambda^* = 2$.

Table 1
Parameter selection.

Parameter	Range
α	(0, 18]
β	(0, 20]
γ	(0, 1]
λ	[1.25, ∞)

According to the analysis of the root locus, it can be concluded that all the eigenvalues can hold real parts and thus the closed-loop system keeps stable by selecting suitable gains. As α, β, and γ increase or λ decreases, the system moves toward the unstable region, making the system oscillatory and eventually leading to instability. There is a sufficient range to design a controller satisfying the requirements of stability and desired dynamics. Though the presented parameter range might not be suitable for different wind farms, the derivation of the linearized model and stability analysis method can still be used for other wind farms.

6. Simulation results

In this section, the effectiveness of the proposed DCVCS is validated under normal and emergency conditions. The wind farm is connected to the IEEE-14 bus system at Bus 05 through a 10-km transmission line as shown in Fig. 5. The communication network is shown in Fig. 4. The test system with the proposed distributed controller is simulated in Matlab/SIMULINK. The wind condition modeling of the wind farm considering the wake effects and turbulence was generated using the SimWindFarm Toolbox [33].

The voltage reference is set as 1.0 p.u. and the control parameters are selected as $\alpha_i = 1$, $\beta_i = 1$, $\gamma_i = 1$, and $\lambda_i = 2$, $\forall\ i \in \mathscr{I}$. The control performance of the proposed DCVCS is compared with the commonly used PI control scheme [7,8], in which reactive power is calculated based on the voltage at the POC and then dispatched to all WTs based on the proportional distribution. The PI controller parameters are designed as $k_p = 10$ and $k_i = 100$.

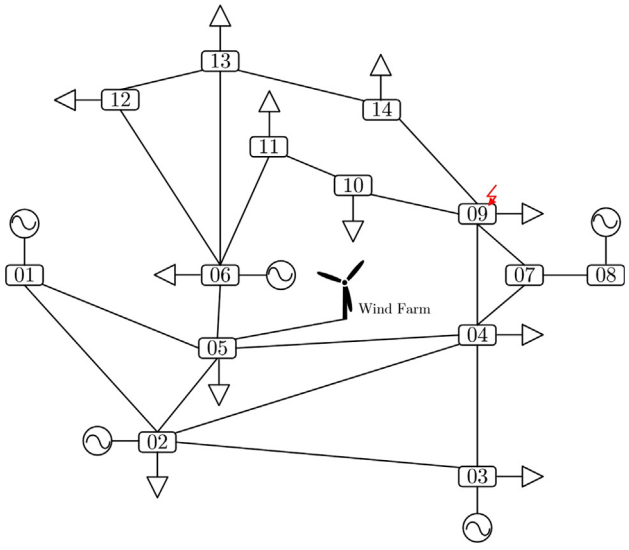

Fig. 5. IEEE-14 bus system with the wind farm.

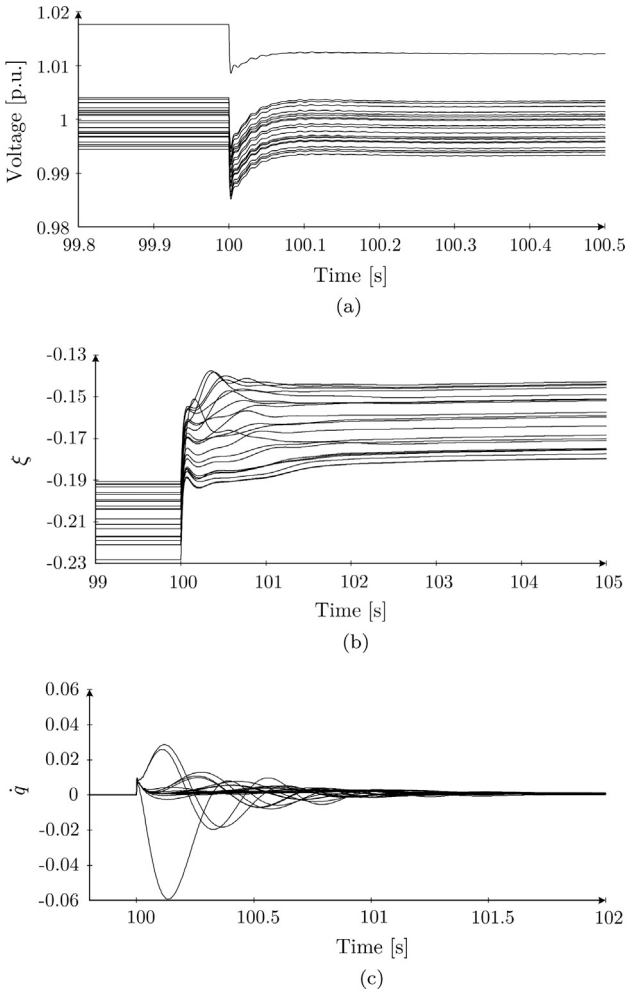

Fig. 6. Convergence performance. (a) Voltage; (b) Reactive power utilization ratio; (C) $\dot{q}$.

6.1. Convergence performance

The convergence of the proposed method is demonstrated in this subsection. To better illustrate the convergence process, a static condition is created by setting constant active power outputs of WTs and loads in external grids. At $t = 100$ s, a additional load is suddenly connected to Bus 05 as a disturbance. The convergence process after the disturbance is shown in Fig. 6. As can be seen, after the disturbance the voltages suddenly drop. Then, the WTs and STATCOM are controlled to provide reactive power support to help the voltage recovery. Finally, after the dynamic process reaches a new equilibrium ($\dot{q} = 0$), which exactly demonstrates the fast convergence of the proposed method.

6.2. Normal operation

In this subsection, the control performance under normal operation is tested. The disturbances are from the active power output variations of WTs and load variations in the external grid. For active power control, WTs are assumed to operate in the Maximum Power Point Tracking (MPPT) mode. The total simulation time is set as 300 s. The simulation results are shown in Fig. 7.

As can be seen from Fig. 7, the voltage at the POC will be lower than 0.95 p.u. during 200−250 s without control and several WT terminal voltages approach to 0.9 p.u.. Thus, the WTs have a risk of being tripped. PI control can effectively regulate the voltage at the POC but it fails to maintain voltages at WT buses within the feasible range (the WT bus voltages reach up to 1.1 p.u.). However, the proposed DCVCS is

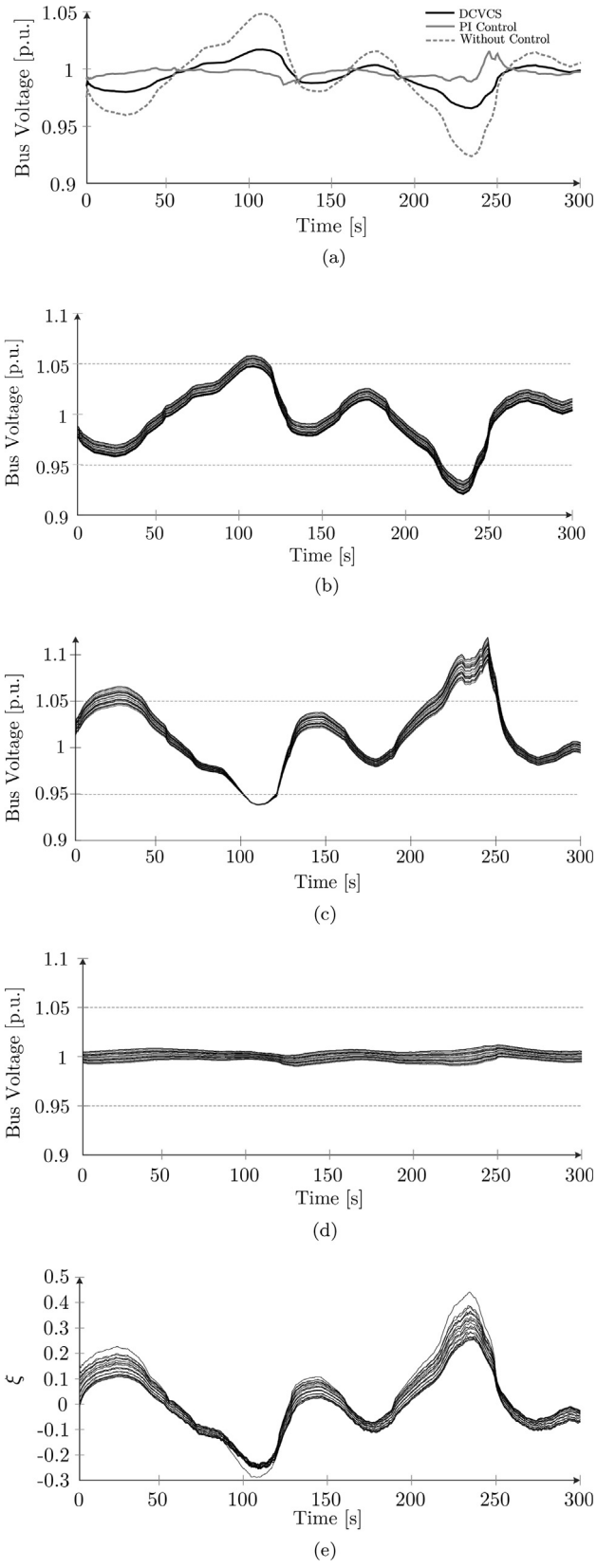

Fig. 7. Control performance under normal operation. (a) Voltage at POC; (b) Terminal voltages of WTs without control; (c) Terminal voltages of WTs with PI control; (d) Terminal voltages of WTs with DCVCS; (e) Reactive power sharing.

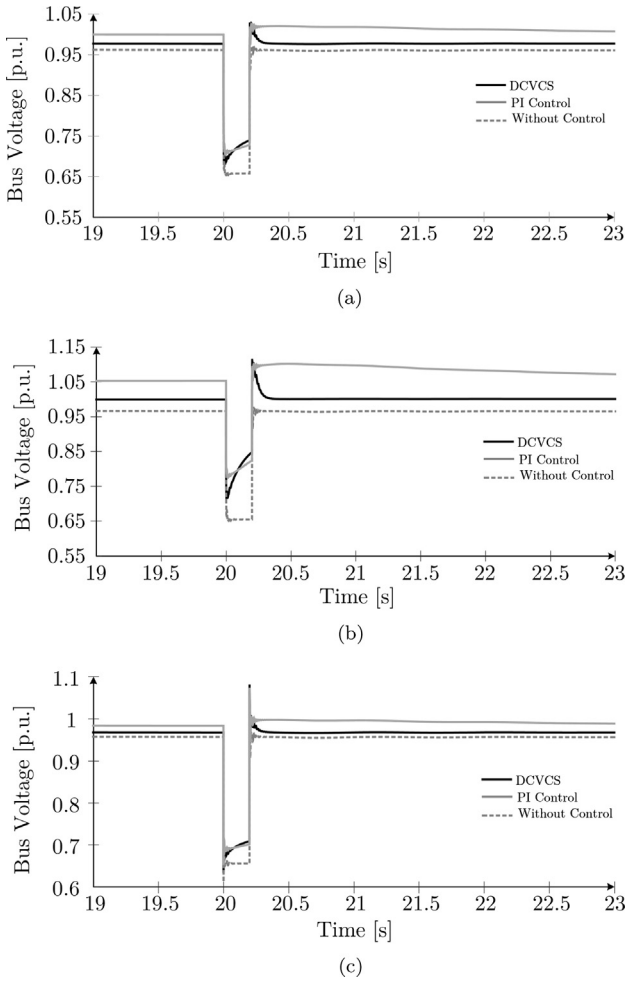

Fig. 8. Control performance under fault-ride-through operation. (a) Voltage at POC; (b) Terminal voltage of WT08; (c) Voltage at Bus05.

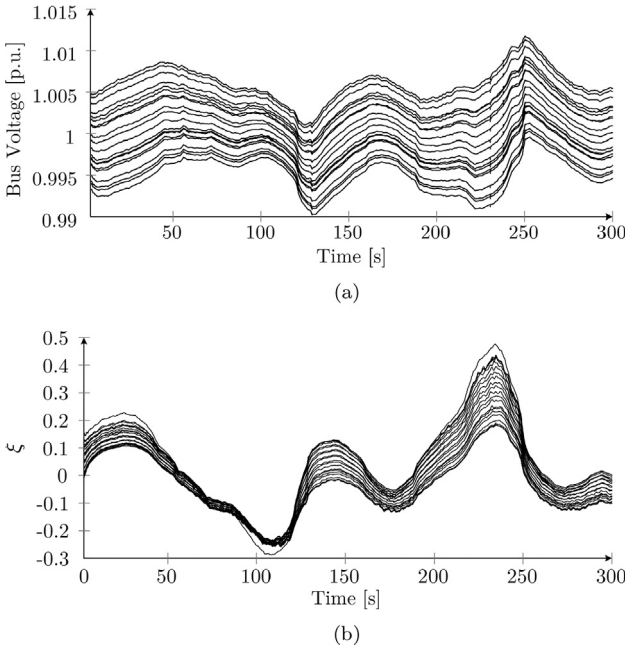

Fig. 9. Control performance under communication link failure. (a) Voltage performance (b) Reactive Power sharing.

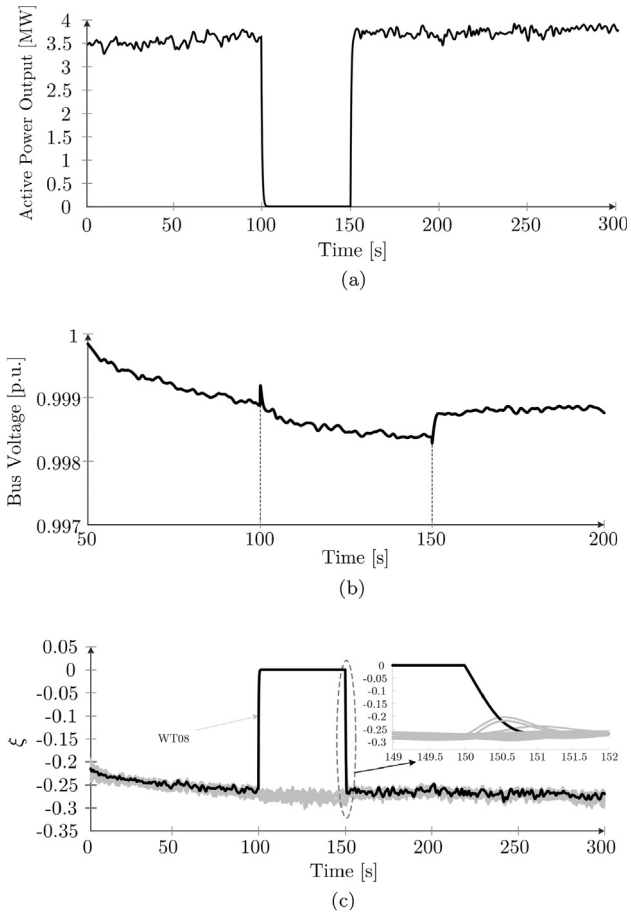

Fig. 10. Control performance under plug-and-play operation. (a) Active power output of WT08; (b) Terminal voltage of WT08; (c) Reactive power sharing.

able to effectively regulate all the network voltages within the feasible range [0.95, 1.05] p.u.. Particularly, the terminal voltages of WTs can be effectively regulated within [0.99, 1.01] p.u., implying better control performance than the PI control.

Fig. 7(e) shows that all the WTs and STATCOM have similar (uniform) reactive power utilization ratio, indicating that the proposed DCVCS can regulate the voltages while keeping fair reactive power sharing.

6.3. Fault-ride-through operation

In this subsection, the control performance under FRT operation is tested. A three-phase short-circuit fault at Bus09 is considered in the case, which occurs at $t = 20$ s and is cleared at $t = 20.2$ s. The simulation results are shown in Fig. 8. As can be seen from Fig. 8, the DCVCS can better help voltage recovery during the fault by taking full use of the reactive power capability of WTs and STATCOM. This could be helpful to prevent the WTs from being tripped by the low-voltage protection during the FRT operation. Besides, it can be concluded that the wind farm can provide reactive power support for the external system, implying that the proposed voltage controller can improve the voltage stability of the system.

6.4. Robustness against communication failure

In this subsection, the robustness of the proposed DCVCS against a communication link failure is tested. The communication link between WT07 and WT08 fails at $t = 100$ s. As shown in Fig. 9, the DCVCS can still provide the similar control performance as presented in the

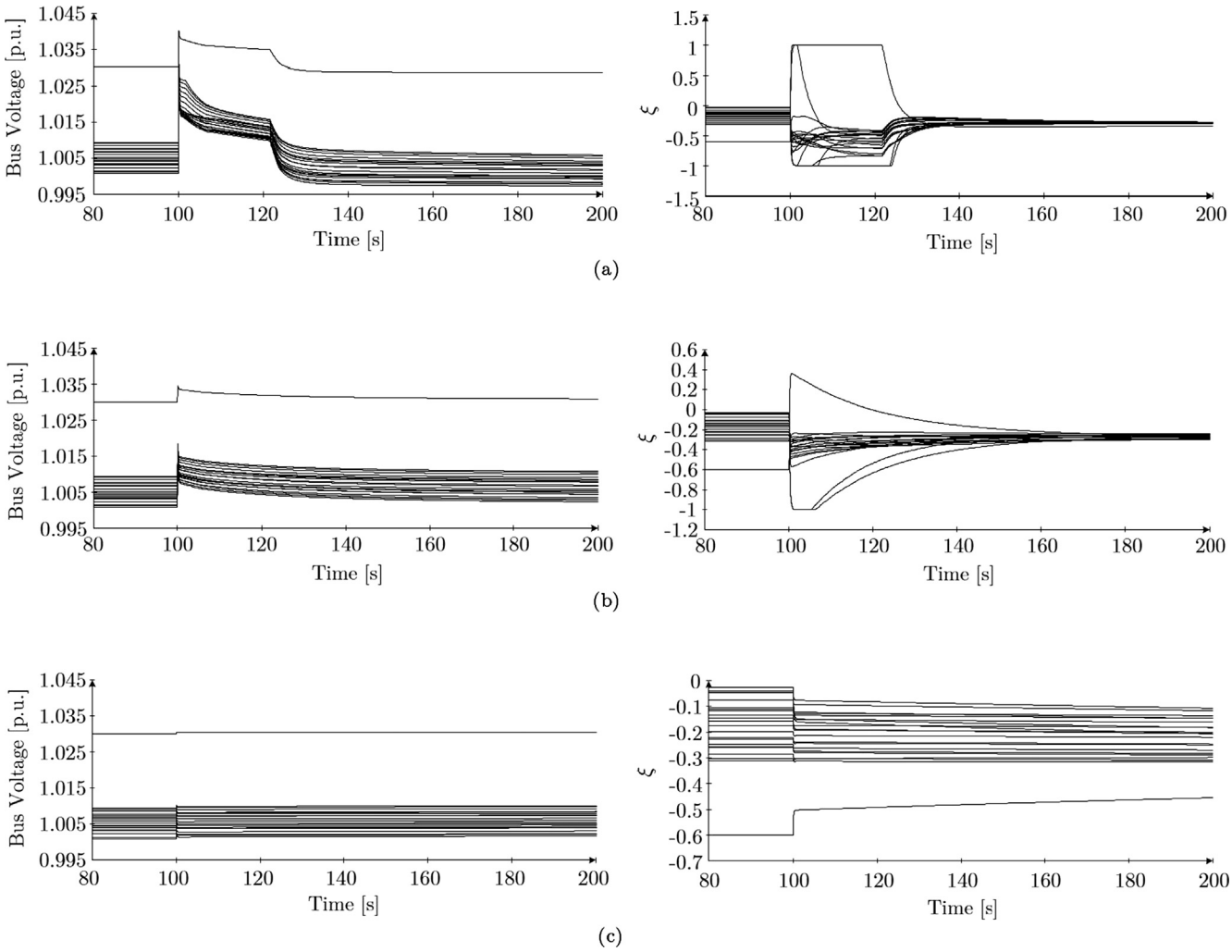

Fig. 11. Control performance under different λ. (a) $\lambda = 10$; (b) $\lambda = 100$; (c) $\lambda = 1000$.

SubSection 6.1 despite the communication link failure between WT07 and WT08, implying good robustness. It is because the communication network of the wind farm is still a connected graph after the communication failure due to the robust communication network design. It might affect the dynamics of the system but the convergence of the consensus protocol is still guaranteed.

6.5. Plug-and-play capability

The plug-and-play capability of the proposed controller is examined in this subsection. WT08 is disconnected at $t = 100$ s and reconnected at $t = 150$ s. As can be seen from Fig. 10, the disconnection and reconnection of WT08 lead to minor disturbances on the system. The proposed controller is able to fast correct voltages and maintain fair reactive sharing after the WT disconnects or reconnects, implying good plug-and-play capability. Comparably, for the centralized control, any change of the wind farm, such as disconnection/reconnection of WTs or extension of wind farm, will result in the modification of the central controller, indicating less flexibility.

6.6. Influence of parameters

In this subsection, the influence of different parameters on control performance is examined. First, the influence of parameter λ is investigated, which affects the system dynamics. Then, the tradeoff between the voltage regulation and reactive power sharing is analyzed by selecting different α, β and γ. To better illustrate the influence of the parameters, only the primary controller is running up to $t = 100$ s, at which time, the secondary voltage controller is activated at $t = 100$ s. Moreover, similar with convergence analysis, the constant active power of WTs and external loads are considered.

6.6.1. Influence of λ

The control performances with different λ are compared, as illustrated in Fig. 11. As can be seen, the smaller λ which means larger gain, can lead to the faster system dynamics and therefore the system reaches to the new equilibrium faster (faster convergence) but might cause system oscillation. A few of reactive sources reach to their reactive power limits during a certain period due to the larger gain.

6.6.2. Influence of α, β and γ

The parameters α, β and γ affect the tradeoff between voltage regulation and reactive power sharing. To demonstrate this, three different modes are designed: 1) pure voltage regulation mode ($\alpha = \beta = 1, \gamma = 0$); 2) Pure reactive power sharing mode ($\alpha = \beta = 0, \gamma = 1$); 3) Compromised mode ($\alpha = \beta = 1, \gamma = 0.2$). As shown in Fig. 12, when $\gamma = 0$ (pure voltage regulation), the WT terminal voltages are tightly regulated around the reference but several units reach up to their reactive power limits and the reactive power sharing is poor. Conversely, in the pure reactive power sharing mode, with no attempt at voltage regulation, the bus voltages are over the reference while the reactive power is shared accurately. In the

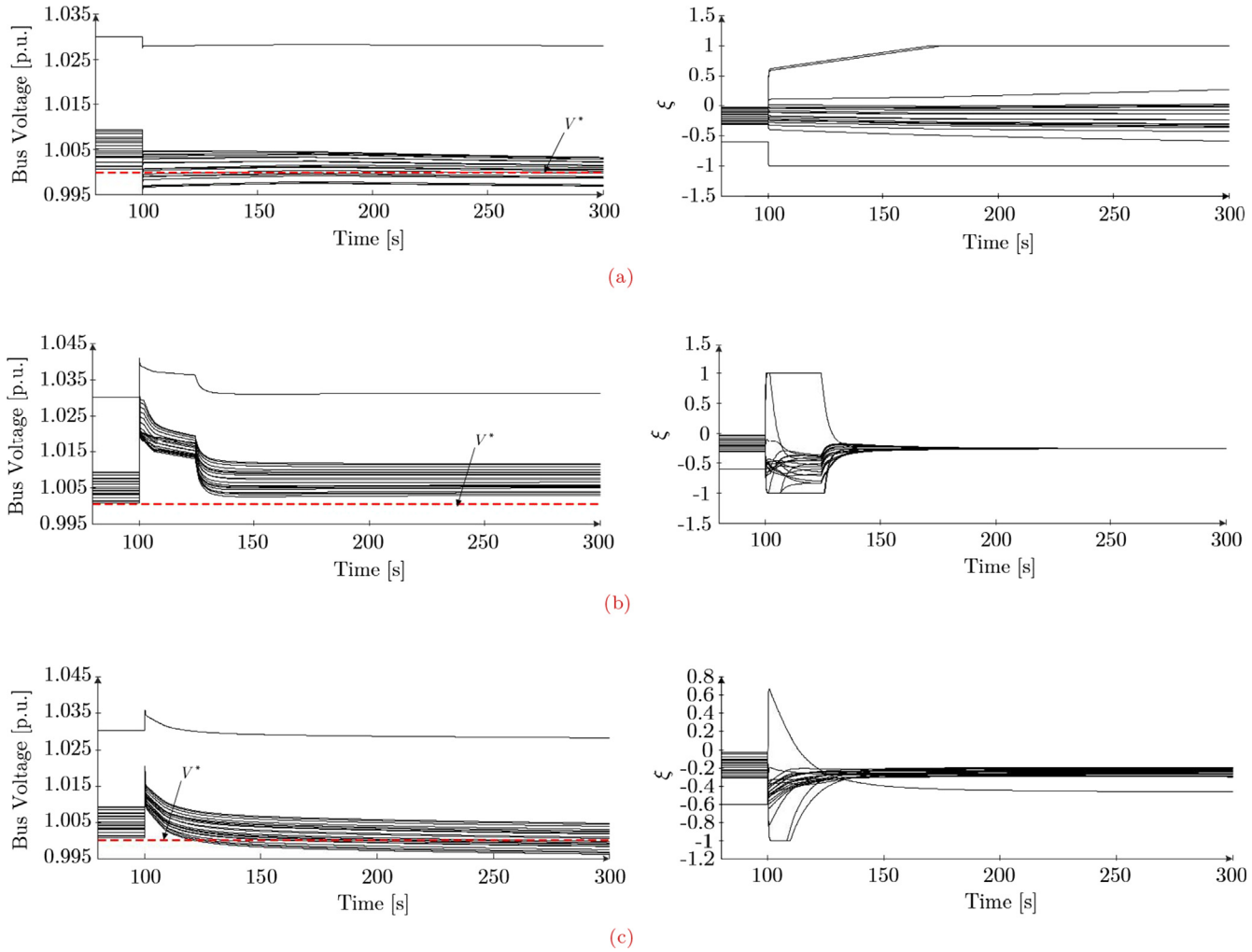

Fig. 12. Reactive utilization ratio. (a) Pure voltage regulation mode ($\alpha = \beta = 1$, $\gamma = 0$); (b) Pure reactive power sharing mode ($\alpha = \beta = 0$, $\gamma = 1$); (c) Compromised mode ($\alpha = \beta = 1$, $\gamma = 0.2$).

compromised mode, the system achieves a compromise between voltage regulation and reactive power sharing.

7. Conclusion

This paper proposes a distributed cooperative voltage control scheme for a wind farm. A droop-based control is adopted as the primary voltage control only based on the local measurements. Then, a distributed cooperative secondary voltage control is developed based on the consensus protocol, which regulates the voltage profile while maintaining fair reactive power sharing. The simulation results show that the proposed controller has good control performance under normal operation and can provide reactive power support under FRT operation. Moreover, the proposed controller has good robustness against the communication link failure and good plug-and-play capability. Compared with the centralized control, the proposed distributed control scheme is more suitable for large-scale wind farms in the near future due to its flexibility and economic benefits. In the future work, the nonlinear stability analysis should be addressed to better investigate the impact of different controller parameters and therefore, the desired system dynamics can be better achieved.

8. Appendix

The sub-matrixes of the matrixes A and B are presented as follows:

$$A_{11} = -\tau_m^{-1}[\tau_Q]^{-1}(\tau_m I_{N_S} + [\tau_Q]) \in \mathbb{R}^{N_S \times N_S},$$
$$A_{12} = -\tau_m^{-1}[\tau_Q]^{-1}(I_{N_S} - [K]\underline{B}_{SS}^{-1}[V_S^0]^{-1}) \in \mathbb{R}^{N_S \times N_S},$$
$$A_{13} = [\tau_Q]^{-1} \in \mathbb{R}^{N_S \times N_S},$$
$$A_{14} = \tau_m^{-1}[\tau_Q]^{-1} \in \mathbb{R}^{N_S \times N_S},$$
$$A_{32} = \tau_m^{-1}[\lambda]^{-1}(([\alpha] + [\beta]\mathscr{L})\underline{B}_{SS}^{-1}[V_S^0]^{-1} + [\gamma]\mathscr{L}[\overline{Q}]^{-1}) \in \mathbb{R}^{N_S \times N_S},$$
$$A_{33} = \tau_m^{-1} I_{N_S} \in \mathbb{R}^{N_S \times N_S},$$
$$B_{11} = -\tau_m^{-1}[\tau_Q]^{-1}[K] \in \mathbb{R}^{N_S \times N_S},$$
$$B_{12} = -\tau_m^{-1}[\tau_Q]^{-1}[K]\underline{B}_{SS}^{-1}\underline{B}_{SK} \in \mathbb{R}^{N_S \times N_K},$$
$$B_{31} = -\tau_m^{-1}[\tau_Q]^{-1}[\alpha] \in \mathbb{R}^{N_S \times N_S},$$
$$B_{32} = \tau_m^{-1}[\tau_Q]^{-1}([\alpha] + [\beta]\mathscr{L})\underline{B}_{SS}^{-1}\underline{B}_{SK} \in \mathbb{R}^{N_S \times N_K}.$$

Acknowledgment

This work is supported in part by the National Key Research and Development Program of China (2016YFB0900603), in part by the Taishan Scholar Program and in part by the China Scholarship Council (CSC).

References

[1] Global Wind Energy Council. Global Wind Statistics 2017; Feb. 2018.
[2] Global Wind Energy Council. Global Wind Report 2016 (GWEC, 2016). 1–73.
[3] Xu L, Yao L, Sasse C. Grid integration of large DFIG-based wind farms using VSC transmission'. IEEE Trans Power Syst 2007;22(3):976–84.

[4] Guo Y, Gao H, Wu Q. A Combined reliability model of VSC-HVDC connected offshore wind farms considering wind speed correlation'. IEEE Trans Sustainable Energy 2017;8(4):1637–46.
[5] Mohseni M, Islam SM. Review of international grid codes for wind power integration: diversity, technology and a case for global standard. Renew Sustainable Energy Rev 2012;16:3876–90.
[6] European Commission. COMMISSION REGULATION (EU) 2016/1447 of 26 August 2016 establishing a network code on requirements for grid connection of high voltage direct current systems and direct current-connected power park modules. Off. J. Eur. Union.; 2016. p. 1–65.
[7] Karthikeya BR, Schutt RJ. Overview of wind park control strategies. IEEE Trans Sustainable Energy 2014;5(2):416–22.
[8] Hansen AD, Sensen PE, Iov F, et al. Centralised power control of wind farm with doubly fed induction generators. Renew Energy 2006;31(7):935–51.
[9] Guo Q, Sun H, Wang B, et al. Hierarchical automatic voltage control for integration of large-scale wind power: design and implementation. Electr Power Syst Res 2015;120:234–41.
[10] Zhao H, Wu Q, Guo Q, et al. Coordinated voltage control of a wind farm based on model predictive control. IEEE Trans Sustainable Energy 2016;7(4):1440–51.
[11] Zhao H, Wu Q, Wang J, Liu Z, et al. Combined active and reactive power control of wind farms based on model predictive control. IEEE Trans Energy Convers 2017;32(3):1177–87.
[12] Schönleber K, Collados C, Pinto RT, et al. Optimization-based reactive power control in HVDC-connected wind power plants. Renew Energy 2017;109:500–9.
[13] Sakamuri JN, Rather ZH, Rime J, et al. Coordinated voltage control in offshore HVDC connected cluster of wind power plants. IEEE Trans Sustainable Energy 2016;7(4):1592–601.
[14] Guo Y, Gao H, Wu Q. Enhanced voltage control of VSC-HVDC connected offshore wind farms based on Model Predictive Control. IEEE Trans Sustainable Energy 2018;9(1):474–87.
[15] Guo Y, Gao H, Wu Q, et al. Coordianted voltage control scheme for VSC-HVDC connected wind farm plants. IET Renew Power Gener 2018;9(1):474–87.
[16] Qin N, Bak KC, Abildgaard H. Automatic voltage control system with market price employing large wind farms. Electr Power Syst Res 2018;157:93–105.
[17] Antoniadou-Plytaria KE, Kouveliotis-Lysikatos IN, Georgilakis PS, et al. Distributed and decentralized voltage control of smart distribution networks: models, methods, and future research. IEEE Trans Smart Grid 2017;8(6). 3999–3008.
[18] Yazdanian M, Mehrizi-Sani A. Distributed control techniques in microgrids. IEEE Trans Smart Grid 2014;5(6):2901–9.
[19] Xin H, Lu Z, Liu Y. A center-free control strategy for the coordination of multiple photovoltaic generators. IEEE Trans Smart Grid 2014;5(3):1262–9.
[20] Xin H, Liu Y, Qu Z, et al. Distributed control and generation estimation method for integrating high-density photovoltaic systems. IEEE Trans Energy Convers 2014;29(4):988–96.
[21] Yorino N, Zoka Y, Watanabe M, Kurushima T. An optimal autonomous decentralized control method for voltage control devices by using a multi-agent system. IEEE Trans Power Syst Sep. 2015;30(5):2225–33.
[22] Liu HJ, Shi W, Zhu H. Decentralized dynamic optimization for power network voltage control. IEEE Trans Signal Inf Process Over Networks Sep. 2017;3(3):568–79.
[23] Dehkordi NM, Sadati N, Hamzeh M. Fully distributed cooperative secondary frequency and voltage control of islanded microgrids. IEEE Trans Energy Convers 2017;32(6):675–85.
[24] Lou G, Gu W, Xu Y, et al. Distributed MPC-based secondary voltage control scheme for autonomous droop-controlled microgrids. IEEE Trans Sustainable Energy 2017;8(2):792–804.
[25] Zhao Y, Chai J, Sun X. Relative voltage control of the wind farms based on the local reactive power regulation. Energies 2017;10(3).
[26] Martínez J, Kjr PC. Fast voltage control in wind power plants. Power and energy society general meeting. 2011. p. 1–7.
[27] Gryning MPS, Wu Q, Kocewiak Ł, et al. Stability boundaries for offshore wind park distributed voltage control. IEEE Trans Control Syst Technol 2017;25(4):1496–504.
[28] Zhao H, Wu Q, Guo Q, et al. Distributed model predictive control of a wind farm for optimal active power controlpart II: Implementation with clustering-based piecewise affine wind turbine model. IEEE Trans Sustainable Energy 2015;6(3):840–9.
[29] Baros S, Ilić MD. Distributed torque control of deloaded wind DFIGs for wind farm power output regulation. IEEE Trans Power Syst 2017;32(6):4590–9.
[30] Baros S, Ilić MD. Distributed Consensus Control of DFIGs with Storage for Wind Farm Power Output Regulation. Available at:http://dspace.mit.edu/handle/1721.1/104796.
[31] Anaya-Lara O, Campos-Gaona D, Moreno-Goytia E, Adam G. Offshore wind energy generation: control, protection, and integration to electrical systems. John Wiley & Sons; 2014.
[32] Jonkman J, Butterfield S, Musial W, Scott G. Definition of a 5-MW reference wind turbine for offshore system development (No. NREL/TP-500-38060). Golden, CO, USA: National Renewable Energy Lab. (NREL); 2009.
[33] Grunnet JD, Soctani M, Knudsen T, Kragelund M, Bak T. Aeolus toolbox for dynamic wind farm model, simulation and control. Proc. eur. wind energy conf. exihib., Warsaw, Poland. 2010. p. 1–10.
[34] Li S, Xu L, Haskew TA. Control of VSC-based STATCOM using conventional and direct-current vector control strategies. Int J Electr Power Energy Syst 2013;45(1):175–86.
[35] Olfati-Saber R, Murray RM. Consensus problems in networks of agents with switching topology and time-delays. IEEE Trans Autom Control 2004;49(9):1520–33.
[36] Hou P, Hu W, Chen Z. Offshore substation locating in wind farms based on prim algorithm. In: Proc. IEEE power energy soc. gen. meet.; 2015. p. 1–5.